The Cryosphere Discussions

The Potsdam Parallel Ice Sheet Model (PISM-PIK) – Part 2: Dynamic equilibrium simulation of the Antarctic ice sheet

M. A. Martin[1,2], R. Winkelmann[1,2], M. Haseloff[1,3], T. Albrecht[1,2], E. Bueler[4], C. Khroulev[5], and A. Levermann[1,2]

[1]Earth System Analysis, Potsdam Institute for Climate Impact Research, Potsdam, Germany
[2]Institute of Physics, Potsdam University, Potsdam, Germany
[3]Dept. of Physics, Humboldt-University, Berlin, Germany
[4]Dept. of Mathematics and Statistics, University of Alaska, Fairbanks, USA
[5]Geophysical Institute, University of Alaska, Fairbanks, USA

Correspondence to: A. Levermann (anders.levermann@pik-potsdam.de)

TCD

4, 1307–1341, 2010

PISM-PIK – Part 2

M. A. Martin et al.

Title Page

Abstract	Introduction
Conclusions	References
Tables	Figures

|◄ | ►|
◄ | ►
Back | Close

Full Screen / Esc

Printer-friendly Version

Interactive Discussion

PISM-PIK – Part 2

M. A. Martin et al.

Abstract

We present a dynamic equilibrium simulation of the ice sheet-shelf system on Antarctica with the Potsdam Parallel Ice Sheet Model (PISM-PIK). The simulation is initialized with present-day conditions for topography and ice thickness and then run to
5 steady state with constant present-day surface mass balance. Surface temperature and basal melt distribution are parameterized. Grounding lines and calving fronts are free to evolve, and their modeled equilibrium state is compared to observational data. A physically-motivated dynamic calving law based on horizontal spreading rates allows for realistic calving fronts for various types of shelves. Steady-state dynamics including
10 surface velocity and ice flux are analyzed for whole Antarctica and the Ronne-Filchner and Ross ice shelf areas in particular. The results show that the different flow regimes in sheet and shelves, and the transition zone between them, are captured reasonably well, supporting the approach of superposition of SIA and SSA for the representation of fast motion of grounded ice. This approach also leads to a natural emergence of
15 streams in this new 3-D marine ice sheet model.

1 Introduction

One of the most severe shortcomings of the Fourth Assessment Report (AR4) of the Intergovernmental Panel on Climate Change (IPCC) was the lack of a process-based assessment of future sea-level rise for the 21st century and beyond. While the direct
20 effect of oceanic warming and related thermal expansion are captured with some uncertainty by state-of-the-art climate models, modeling studies for fast processes in land ice continue to be sparse. Observations, however, support the importance of modeling these ice flow processes. On the Antarctic Peninsula, for example, an acceleration of ice flow across the grounding line has been observed in response to ice-shelf disin-
25 tegration (e.g., Pritchard et al., 2009). The fast ice flow regimes in the vicinity of the grounding line as well as ice-shelf dynamics constitute two of the largest challenges in ice sheet modeling.

M. A. Martin et al.

Here we present a simulation for the Antarctic sheet-shelf system with the Potsdam Parallel Ice Sheet Model (PISM-PIK) with a special focus on both ice shelf dynamics and the transition zone between grounded and floating ice.

Our modeling approach is based on the Shallow Ice Approximation (SIA) and the Shallow Shelf Approximation (SSA) which make use of the fact that ice thickness is small compared to relevant horizontal scales and reduce the full Stokes problem by scaling the equations with the small depth-to-width ratio of ice sheets. There are several models combining the stress balance from the SIA for grounded ice with the SSA for ice shelves in simulations of the Antarctic Sheet-Shelf system (e.g., Huybrechts, 1990; Hulbe and MacAyeal, 1999; Ritz et al., 2001; Pollard and Deconto, 2009). Based on the Parallel Ice Sheet Model (PISM, Bueler and Brown, 2009), the Potsdam Parallel Ice Sheet Model (PISM-PIK) introduced additional components which are particularly relevant for ice shelf dynamics (Winkelmann et al., 2010). These include a stress boundary condition, a parameterization for subgrid-scale motion of ice-shelf calving-fronts (Albrecht et al., 2010) and a new calving-rate law which is presented in Levermann et al. (2010).

In this paper we first describe the set-up for a dynamic equilibrium simulation for Antarctica in Sect. 2. Section 3 presents a dynamic equilibrium simulation for Antarctica under present-day conditions performed with PISM-PIK and summarizes and discusses the performance of PISM-PIK in comparison with observations. A conclusion is given in Sect. 4.

2 Model setup for the dynamic equilibrium simulation

Our dynamic equilibrium simulation used the following model setup:

The model domain is discretized on a 301×301 horizontal grid with 19.98 km spacing. The vertical grid has 51 levels within a domain extending 5000 m above the bed elevation. The vertical spacing ranges from 26.5 m in the lowest layer to 173.5 m spacing at the surface of the thickest ice. The temperature is stored on this unequally-spaced

PISM-PIK – Part 2

M. A. Martin et al.

grid, but the equation of conservation of energy is solved on a vertical grid with uniform spacing of 26 m. A thin bedrock layer of 265 m with 26.5 m spacing was used, following the reasons given in Bueler and Brown (2009).

The input fields for topography and initial ice thickness are regridded from the present-day ALBMAP v1 data (Le Brocq et al., 2010) available on the (SeaRISE) Project website. These data update the earlier BEDMAP (Lythe et al., 2001). Surface mass balance was adopted from Van de Berg et al. (2006), and geothermal flux is based on the model of Shapiro and Ritzwoller (2004). Throughout the equilibrium simulation surface mass balance, geothermal flux and topography are held fixed. Notation for this paper is in Table 1.

With this input data, shelves are determined by applying the flotation criterion:

$$b(x,y) \leq -\frac{\rho_i}{\rho_o} H(x,y) \,. \tag{1}$$

Similar to Huybrechts (1993) and Pollard and Deconto (2009), the surface temperature field is parameterized as a function of latitude and surface elevation. For surface elevations above $h=100$ m we use

$$T_s = 273.15 + 30.7 - 0.0081h - 0.6878|\Phi| \tag{2}$$

with latitude $|\Phi|$ in $^\circ$S, temperature is given in Kelvin. In order to avoid too low temperatures on the ice shelves compared to observations, the dependence on surface elevation is dropped below 100 m, where we use:

$$T_s = 273.15 + 29.89 - 0.6878|\Phi| \quad \text{for} \quad h < 100 \text{ m} \,. \tag{3}$$

Note that 87% of the ice area with surface elevations below 100 m consists of ice shelves. This parameterization reproduces the observed temperatures for the present-day surface elevation (Comiso, 2000; Van den Broeke, 2008) particularly on the ice shelves.

For the base of the ice shelf, the pressure-melting temperature T_{pm} is applied as a boundary condition for the temperature evolution within the ice:

$$T_{pm} = 273.15 + \beta_{CC} z_b \qquad (4)$$

with z_b as the elevation (generally negative) of the base of the ice shelf and with
5   Clausius-Clapeyron gradient β_{CC}. This pressure-melting temperature for meteoric ice is distinct from the freezing temperature of saline ocean water T_f at this depth

$$T_f = 273.15 + 0.0939 - 0.057 S_o + 7.64 \times 10^{-4} z_b \qquad (5)$$

which is used for the calculation of the heat flux between ice shelf and ocean (Beckmann and Goosse, 2003). Here S_o is the salinity of the ocean which we set to an
10   average value of 35 psu. The resulting heat flux between ocean and ice is computed from

$$Q_{heat} = \rho_o c_{p_o} \gamma_T F_{melt} (T_o - T_f) \qquad (6)$$

based on Holland and Jenkins (1999), with ρ_o density of ocean water and c_{p_w} specific heat capacity of the ocean mixed layer in which salinity changes from close to zero
15   near the base of the ice (Oerter et al., 1992) to a value around 35 psu in the ocean. Here γ_T is the thermal exchange velocity and F_{melt} a model parameter. For the present simulation T_o is set to a constant value of $-1.7\,°C$ (see Table 1), based on the NCEP reanalysis value for the Ross Ice Shelf given in Beckmann and Goosse (2003). The heat flux is not used as a temperature boundary condition on the ice but is transformed
20   into a mass flux S from shelf to ocean through

$$S = Q_{heat}/(L_i \rho_i) \qquad (7)$$

where L_i is the latent heat capacity of ice and ρ_i ice density. This results in a spatial distribution of subshelf melt rates depending on the shelf bottom temperature which is closely related to the shelf thickness (Fig. 1).
25   As detailed in Winkelmann et al. (2010), ice velocities are calculated in PISM-PIK as a direct superposition of the SIA and the SSA velocities computed everywhere in the

Title Page

Abstract | Introduction

Conclusions | References

Tables | Figures

◄◄ | ►►

◄ | ►

Back | Close

Full Screen / Esc

Printer-friendly Version

Interactive Discussion

PISM-PIK – Part 2

M. A. Martin et al.

grounded ice. In fact, for grounded ice the SSA velocity is interpreted as the basal sliding velocity v_b (Bueler and Brown, 2009). This provides a smooth transition both from non-sliding ice which is frozen to the bedrock to an ice stream where sliding occurs, and from rapidly-sliding ice which flows across the grounding line into an ice shelf.

5 Compared to PISM we avoid a weighting function when combining the two velocity contributions. Streams are defined diagnostically as regions where SSA (i.e. basal) velocities v_b are larger than SIA velocities,

$$v_b > \bar{v} - v_b \tag{8}$$

with $\bar{v}$ the vertical average of the full velocity $v_{SIA} + v_{SSA}$.

10 The idea of superposing the two shallow approximations and defining streams as above is supported by analytic calculations for the flow line case (Schoof and Hindmarsh, 2010). Figure 2 shows the emerging velocity patterns for an exemple cut through the sheet-shelf transition zone of the Lambert Glacier and the Amery Ice Shelf in the simulation. This example illustrates how the two velocity contributions supersede

15 each other except in a transition region in the upper part of an ice stream. The onset of an ice stream can be found where the SSA velocity rises above the SIA velocity on grounded ice, i.e. where the red curve crosses the blue curve in Fig. 2. We see that the model is capable of capturing this observed transition to rapid flow upstream of an ice shelf without artificially prescribing any internal boundary conditions within the ice.

20 When aiming at modeling different flow regimes, the isotropic (Glen) flow law used here (Winkelmann et al., 2010) might not be the best choice. Ma et al. (2010) suggest that velocities in the grounded part of an ice sheet are often underestimated by models using such isotropic laws, while they are overestimated in ice shelves. In applying PISM-PIK to the Antarctic sheet-shelf system we adjust for un-modeled anisotropy,

25 and also for other uncertainties relating to unobserved variations in viscosity and basal resistance, by using different enhancement factors for the SIA (E_{SIA}) and the SSA (E_{SSA}), respectively.

Note $E_{SIA} > 1$ and $E_{SSA} < 1$; see Table 1 for values. This difference in quality for the two enhancement factors is justified by the fact that under compression the fabric of ice

becomes axisymmetric and easier to shear than isotropic ice, whereas under tension girdle-type fabrics evolve and make the ice stiffer (Ma et al., 2010). In PISM-PIK we use a uniform enhancement factor for the SSA, but, because the SSA velocity is interpreted as the sliding velocity for grounded ice, the effective flow enhancement arising from the superposition decreases for ice flowing through the transition from sheet to shelf; compare Fig. 2.

Basal friction within the SSA equations, which is crucial for the magnitude of the computed sliding velocities, is calculated based on a model for plastic till (Schoof, 2006a)

$$\tau_{b,i} = -\tau_c \frac{v_i}{\left(v_x^2 + v_y^2\right)^{1/2}} \ , \tag{9}$$

as described in Winkelmann et al. (2010). The basal yield stress τ_c is given by the Mohr-Coulomb model for saturated till with zero cohesion (Paterson, 1994)

$$\tau_c = \tan\phi(\rho_i gH - p_w) \ . \tag{10}$$

Strictly speaking, Eq. (9) only describes the yield stress in a perfectly-plastic basal model. This value of the yield stress is only valid where sliding is occurring. Because the basal stress is computed by a regularized plastic law (Bueler and Brown, 2009, Eq. 27), however, at stresses lower than the yield stress there is a very small amount of sliding on the order of 10 cm/a or less. Comparison to an exact solution to the perfectly-plastic model shows that this regularization indeed has only a small effect (Bueler and Brown, 2009). The designation of "non-sliding-ice" is therefore applied to the vast regions in the interior of the ice sheet with such negligibly small SSA velocities, recognizing that they would have exactly zero basal sliding in a perfectly-plastic model.

For our simulation of Antarctica, the friction angle ϕ (Clarke, 2005) is parameterized with bed elevation as

$$\phi(x,y) = \begin{cases} 5°\,, & b(x,y) \leq -1000\,, \\ 5° + 15°\left(1 + \frac{b(x,y)}{1000}\right)\,, & -1000 < b(x,y) < 0\,, \\ 20°\,, & 0 \leq b(x,y) \end{cases} \qquad (11)$$

The pore water pressure

$$p_w = 0.96\rho_i gH\lambda \qquad (12)$$

is limited to a maximum of 96% of the overburden pressure $\rho_i gH$ for maximal λ, i.e. for ice resting on bedrock at or below sea level. The scaling parameter λ, given by

$$\lambda(x,y) = \begin{cases} 1\,, & b(x,y) - z_{sl} \leq 0\,, \\ \left(1 - \frac{b(x,y) - z_{sl}}{1000}\right) & 0 < b(x,y) - z_{sl} < 1000\,, \\ 0\,, & 1000 \leq b(x,y) - z_{sl}\,, \end{cases} \qquad (13)$$

ranges, depending on sea level z_{sl} and bed elevation, from 0 to 1. It can be interpreted as water content in the till. Bueler et al. (2010) and Bueler and Brown (2009), using base PISM, compute this water content thermodynamically from the basal melt rate, but our simpler parameterization results in a pressure distribution which is similar to the thermodynamically-computed result. Effective pressure varies linearly between 4% of overburden pressure in marine areas and full overburden where the bed exceeds 1000 m above sea level. For simplicity and in order to focus here on the ice dynamics we choose to use a basal friction parameterization for the presented simulation according to Eqs. (9–13), which is only dependent on topography and ice thickness. Thus PISM-PIK essentially models full water content ($\lambda=1$) uniformly in marine areas, which is crucial for the development of streams as illustrated, for example, in Fig. 10. More data about the conditions at the base of the ice would be needed to precisely model the locations and velocities of streams in Antarctica. Inverse modeling (Joughin et al., 2009) would improve the parameterization of basal friction, but basal friction is not the

Title Page

Abstract | Introduction

Conclusions | References

Tables | Figures

◀◀ | ▶▶

◀ | ▶

Back | Close

Full Screen / Esc

Printer-friendly Version

Interactive Discussion

only control mechanism for the structure of streams, as these streams arise from the simultaneous solution of the thermomechanically-coupled SSA and SIA equations.

PISM-PIK incorporates a new physically-motivated treatment of the calving fronts. In fact, following Levermann et al. (2010), calving occurs in regions of divergent flow where both eigenvalues $\dot{\epsilon}_\pm$ of the horizontal strain rate tensor are positive. In such cases we define the calving rate to be

$$C = K \det(\dot{\boldsymbol{\epsilon}}) = K \dot{\epsilon}_+ \dot{\epsilon}_- \quad \text{for} \quad \dot{\epsilon}_\pm > 0 \tag{14}$$

with $K > 0$ being a proportionality constant.

This dynamic calving law allows for realistic calving fronts for various types of shelves, e.g., relatively thin ones like Larsen C with ice thicknesses H_c of about 170–220 m at the calving front as well as for Ross ($H_c \approx 220$–395 m) and Ronne ($H_c \approx 320$–340 m). The new calving law ensures that shelf ice is cut off at the mouth of bays, like the Ross bay, for example.

In Fig. 4 the along-flow eigenvalue $\dot{\epsilon}_+$ for our simulations is illustrated together with the zero lines for the across-flow eigenvalue $\dot{\epsilon}_-$. In most parts, this second eigenvalue is negative, indicating compression within the shelf. Regions where $\dot{\epsilon}_-$ is positive – indicating expansion in the transversal direction – are critical in the sense that once a calving front retreats back to such a position then a new stable calving front position is established. Convergence of ice flow can be produced by pinning points like ice rises, islands or predominant coast features, which stabilize the calving front.

3 Dynamic equilibrium simulation

PISM-PIK as described above was applied to the Antarctic ice-sheet-shelf system in a dynamic equilibrium simulation using time-invariant input data as described in Sect. 2. After initialization with presently-observed fields the model reached an equilibrium with 259×10^{14} m^3 ice volume compared to the 256×10^{14} m^3 deduced from the ALBMAP data set. The first part of the spinup procedure consisted of a 200 000 years model

Title Page

Abstract | Introduction

Conclusions | References

Tables | Figures

◀◀ | ▶▶

◀ | ▶

Back | Close

Full Screen / Esc

Printer-friendly Version

Interactive Discussion

run with fixed geometry and non-evolving surface such that the three-dimensional temperature field within the ice body could evolve according to the conservation of energy equation. Afterwards the dynamic equilibrium simulation using the physical framework described in Winkelmann et al. (2010) ran for 150 000 years using the boundary conditions described in Sect. 2 and the parameter values from Table 1. After this the model is in quasi-equilibrium in the sense that its drift in sea-level relevant ice volume is less than –0.000025% in 1000 years, which is equivalent to an average sea-level rise of $\approx$0.0014 mm/year. (To compute the sea-level-relevant ice volume we reduced the total grounded volume by the amount of ice, that – in liquid form – would fill up the regions with bedrock below sea level, if all ice were removed.) The total ice volume is subject to larger fluctuations which occur on a timescale of decades and are of the same magnitude as this drift shows in 20 000 yr.

Table 2 provides key features and characteristic quantities of Antarctica, comparing the equilibrium state produced in PISM-PIK with observations from the ALBMAP dataset. The steady state reached in the simulation will be further analyzed by considering the geometric configuration (in Sect. 3.1), the mass budget (in Sect. 3.2) and the steady-state dynamics (in Sect. 3.3).

3.1 Geometric configuration in steady state

In PISM-PIK all lateral boundaries are free to evolve: The grounding line, as well as (floating) calving fronts, grounded ice fronts (marine margins), and ice cliffs (ice resting on bedrock above the ocean surface) as shown in Fig. 7. In Fig. 5 we present a comparison, between observation (Lythe et al., 2001; Le Brocq et al., 2010) and simulation, of the position of those lateral boundaries.

The Ross Ice Shelf front as well as the front of the Ronne-Filchner Ice Shelf are well-captured by the applied calving law (Levermann et al., 2010). The position of the front of Larsen C Shelf, which is clearly thinner than the other two shelves is also reproduced by the same calving law. This result cannot be obtained by a simple ice-thickness calving law where floating ice thinner than a certain global threshold value is

Title Page

Abstract	Introduction
Conclusions	References
Tables	Figures

◀◀ ▶▶

◀ ▶

Back Close

Full Screen / Esc

Printer-friendly Version

Interactive Discussion

simply cut off. However, our model resolution of ≈20 km fails to capture a number of the smaller ice shelves that consist of a handfull or fewer grid cells. This is also reflected in the partitioning of ice-front types, which differs from the observational data as shown in Table 2.

5   The simulated grounding line of the Ross Ice Shelf lies further inland than observed. Its position is strongly dependent on topography (via the parameterization of basal resistance, Eqs. 9–13), on the melt rate at the base of the adjacent ice shelf, and on the velocities in the shelf, which in turn are subject to the enhancement factor E_{SSA}. In Fig. 6 modeled surface elevation is given as well as a comparison of ice thickness

10 to observation. The majority of the grid cells show a deviation in ice thickness of not more than a couple of hundred meters (positive or negative, Fig. 6b). The combination of the positive anomalies in the Amery region and directly upstream of the grounding line of the Ross Ice Shelf, the Pine Island Glacier and the Filchner Ice Shelf, and the negative anomaly for the West Antarctic Ice Sheet and large parts of the East Antarctic

15 Ice Sheet explains the total difference of only 1.2% of the total ice volume, $259 \times 10^{14}\,\mathrm{m}^3$ in the simulation as compared to $256 \times 10^{14}\,\mathrm{m}^3$ observed, see Table 2.

     One of the stronger positive deviations in ice thickness occurs in the Amery Shelf area. While the model reproduces the general structure of this region, the outflow here is apparently underestimated, although a strong improvement was achieved by use of

20 the ALBMAP data set by Le Brocq et al. (2010) relative to earlier use of BEDMAP (Lythe et al., 2001) in the model. With some exceptions the ice thickness in the simulation is underestimated along the modeled ice divides, while it is overestimated in the regions of strong outflow (see Fig. 10).

3.2   Mass balance

25 The geometric configuration as described above is determined by the ice fluxes in steady state which are allocated to shelf ice, marine ice and ice grounded above sea-level. The partitioning of the different types of ice cells in the equilibrium simulation is depicted in Fig. 7. Large areas of the West Antarctic Ice Sheet and also of the East

Antarctic Ice Sheet are marine. Depending on the slope of their bed in the ice-flow direction they are subject to the well-known marine ice sheet instability proposed by Weertman (1974). Bamber et al. (2009) give a recent reassessment of this instability for WAIS.

5 In steady state the surface mass balance, which is held constant in the simulation, is balanced by the bottom mass balance (subsheet and subshelf melting and refreezing) and the flux across the ice front. In terms of total mass flux, the bottom mass balance plays a negligible role, while the crucial contribution is the flux across the ice front. The ice front is composed of marine ice cells, cliffs and floating front cells as shown in
10 diagram 8a. For all types of ice fronts, mass loss occurs through calving. In the case of cliffs and marine fronts, this happens through the formation of shelves which are only one grid-box long, which then calve off in the same timestep.

Diagram 8b shows that most of the mass loss occurs at marine ice fronts and shelves. Only a small part occurs at cliffs (about 12%) relative to their extent (24%
15 of the ice front of Antarctica is comprised of cliffs). Conversely, although shelves account for only 22% of the total modeled ice front of Antarctica, they provide 40% of the mass loss. This can be explained by the different magnitude of velocities in sheet and shelves which will be further discussed in Sect. 3.3. Also in regions with high outflux the model tends to produce ice shelves.

20 The formation of shelves influences the grounded ice upstream and thereby the mass balance both by buttressing effects in the case of an embayment and through the drawdown of grounded ice. As shown in Sect. 3.1 there is a smaller total ice shelf area in our simulation than observed. A subgrid treatment of grounded margins analogous to that for the calving fronts, and higher resolution, might improve this.

25 ## 3.3 Steady state dynamics

The ice geometry, grounding line position, ice front position, and ice front type each evolve to an approximate equilibrium at the end of the simulation. In Fig. 9 the surface velocities for this steady state are detailed for the West Antarctic Ice Sheet. In

Fig. 10 the flow pattern for the whole Antarctic ice sheet is shown, with the onset of streams marked by black lines. As described in Sect. 2 streams are (diagnostically) distinguished from the surrounding ice by comparing the sliding velocity $v_b=v_{SSA}$ to the vertically averaged velocity $\bar{v}$: If $v_b>\bar{v}-v_b$ then we consider the flow stream-like.

5   The overall pattern of drainage basins is easily recognizable: for WAIS there is drainage into the Amundsen Sea sector, an area subject to accelerated thinning in reality (Thomas et al., 2004; Pritchard et al., 2009). A feature that can be roughly identified with Thwaites Glacier plays a more prominent role in the flow field of our simulation than Pine Island Glacier. The latter has its grounding line further seaward

10 than in reality. These differences might be due to the ≈20 km resolution in our model. Drainage into the Ronne Shelf occurs from several different basins, both north and south of the Ellsworth mountains. Another prominent feature is the drainage from East Antarctia into the Ross Ice Shelf via the Byrd and Mulock Glaciers. In East Antarctica the main drainage basins can be connected to the marine areas as shown in Fig. 7,

15 indicating the strong influence of bottom topography on our simulation.

    Figure 11 shows the ice flux for the combined stream-shelf system for the two largest shelves. Due to the anomaly in the position of the grounding line the location of the streams does not directly coincide with real streams in Antarctica. Combining the SIA and SSA velocities as described in Sect. 2 is, however, shown to model stream-like

20 features in a reasonable way.

    In order to compare these model results to observational data we combined two sources, namely present-day surface velocities from both the Modified Antarctic Mapping Mission (Jezek et al., 2003; Liu et al., 1999) and for the Siple Coast area of WAIS, from Joughin et al. (2002). The resulting velocity is compared to the modeled surface

25 velocities in Fig. 12. The model magnitudes deviates from observations in some areas, but the overall pattern and distribution of velocities in shelves, streams and areas frozen to the bed is clearly comparable. This is further supported by the scatterplot of velocity magnitudes (Fig. 13), illustrating the close correlation between the modeled and observed velocities. The comparison shows that while the grounded modeled

velocities are in good agreement with observations, the velocities on the shelves are overestimated with a mean difference of ≈330 m/a subject to a high variance (standard deviation ≈280 m/a). The differences vary from shelf to shelf.

A histogram of the velocity distribution is given in Fig. 14. The Antarctic ice sheet has
5   a large number of low-velocity and a small number of high-velocity grid cells. For both simulation and observation we see that the number of grounded grid cells decreases with increasing velocity, while the number of floating grid cells is relatively constant in the low velocity range and then decreases. The histogram in Fig. 15 is based on the subset of observed velocity points shown in Fig. 12 matching the ice type in the simu-
10 lation. A decomposition into grounded and floating regions reveals that high velocities are predominantly found on ice shelves. This also reveals the limitations of PISM-PIK in reproducing the details of the observed velocity distribution: There are more float-ing cells in the quasi-uniformly distributed low-velocity range in observations than our model can reproduce. On the other hand, cells with higher velocities on shelves are
15 too numerous in the simulation, but the strongest overestimation occurs only in a small number of grid cells. For grounded grid cells the model gives more realistic values (see also Fig. 13).

4   Conclusions

Our dynamic equilibrium simulation for Antarctica demonstrates the ability of PISM-PIK
20 to reproduce large-scale dynamic features of the Antarctic ice sheet-shelf system, in-cluding observed features such as streams and the position of ice fronts. A comparison of the geometry and dynamics in modeled equilibrium using observed surface veloc-ities covering ≈65% of the ice-covered area supports the PISM-PIK treatment of the calving front and its direct superposition of SIA and SSA. These new techniques cap-
25 ture ice streams and the full range of fast-flowing ice in the whole sheet/shelf system. This hybrid scheme leads to a smooth transition from sheet to shelves and permits a diagnostic definition of streams (Fig. 2). The mass budget of Antarctica in simulated

PISM-PIK – Part 2

M. A. Martin et al.

Title Page

Abstract | Introduction

Conclusions | References

Tables | Figures

⏮ | ⏭

◀ | ▶

Back | Close

Full Screen / Esc

steady state was analyzed, identifying the composition of mass loss at different types of ice fronts (Fig. 8).

Though subgrid interpolation is used in PISM-PIK for the floating parts of the calving front (Albrecht et al., 2010), it is not currently used for locations where the model has grounded ice margins. This may be the explanation for a reduced area of floating ice in the model relative to observations (Table 2). Noting that the formation of an attached shelf influences the grounded ice upstream, both by buttressing effects in the case of an embayment and the draw-down of grounded ice because of high shelf velocities being transmitted by membrane stresses into the upstream grounded ice, additional subgrid treatment may improve grounded marine margins in future model versions.

Significant additional improvements, particularly with respect to grounding line position (Fig. 5), ice thickness distribution (Fig. 6), and velocity distribution (Figs. 9–15), are expected from finer grid resolution, improved topographic input data, and additional information on the dynamic basal boundary conditions (basal shear stress) of grounded ice.

References

Albrecht, T., Martin, M. A., Winkelmann, R., Haseloff, M., and Levermann, A.: Parametrization for subgrid-scale motion of ice-shelf calving-fronts, The Cryosphere Discuss., submitted, 2010. 1309, 1321

Bamber, J. L., Riva, R. E. M., Vermeersen, B. L. A., and LeBrocq, A. M.: Reassessment of the potential sea-level rise from a collapse of the West Antarctic ice sheet, Science, 324, 901–903, 2009. 1318

Beckmann, A. and Goosse, H.: A parametrization of ice shelf-ocean interaction for climate models, Ocean Modell., 5(2), 157–170, 2003. 1311

Title Page

Abstract | Introduction

Conclusions | References

Tables | Figures

◄ | ►

◄ | ►

Back | Close

Full Screen / Esc

Printer-friendly Version

Interactive Discussion

Bueler, E. and Brown, J.: The shallow shelf approximation as a sliding law in a thermomechanically coupled ice sheet model, J. Geophys. Res., 114, F03008, doi:10.1029/2008JF001179, 2009. 1309, 1310, 1312, 1313, 1314

Bueler, E., Khroulev, C., Aschwanden, A., Joughin, I., and Smith, B.: Modeled and observed fast flow in the Greenland ice sheet,Geophys. Res. Letters, submitted. 1314

Clarke, G. K. C.: Subglacial processes, Ann. Rev. Earth Planet. Sc., 33, 247–276, 2005. 1314

Comiso, J. C.: Variability and trends in Antarctic surface temperatures from in situ and satellite infrared measurements, J. Climate, 13, 1674–1696, 2000. 1310

Holland, D. M. and Jenkins, A.: Modeling thermodynamic ice-ocean interactions at the base of an ice shelf, Journal of Physical Oceanography, 29, 1787–1800, 1999. 1311

Hulbe, C. L. and MacAyeal, D. R.: A new numerical model of coupled inland ice sheet, ice stream, and ice shelf flow and its application to the West Antarctic ice sheet, J. Geophys. Res., 104, 25349–25366, 1999. 1309

Huybrechts, P.: A 3-D model for the Antarctic ice-sheet: a sensitivity study on the glacial-interglacial contrast, Clim. Dynam., 5, 79–92, 1990. 1309

Huybrechts, P.: Glaciological modellint of the late Cenozoic East Antarctic ice sheet: stability or dynamism, Geogr. Ann. A, 75(4), 221–238, 1993. 1310

Jezek, K. C., Farness, K., Carande, R., Wu, X., and Labelle-Hamer, N.: RADARSAT 1 synthetic aperture radar observations of Antarctica: modified antarctic mapping mission, 2000, Radio Sci., 38, 8067–8074, 2003. 1319

Joughin, I., Tulaczyk, S., Bindschadler, R., and Price, S. F.: Changes in West Antarctic ice stream velocities: observation and analysis, J. Geophys. Res., 107, 2289–2311, 2002. 1319, 1338

Joughin, I., Tulaczyk, S., Bamber, J., Blankenship, D., Holt, J., Scambos, T., and Vaughan, D.: Basal conditions for Pine Island and Thwaites Glaciers determined using satellite and airborne data, J. Glaciol., 55, 245–257, 2009. 1314

Le Brocq, A. M., Payne, A. J., and Vieli, A.: Antarctic dataset in netCDF format, doi:10.1594/PANGAEA.734145, http://doi.pangaea.de/10.1594/PANGAEA.734145, 2010. 1310, 1316, 1317, 1326

Levermann, A., Albrecht, T., Winkelmann, R., Martin, M. A., and Haseloff, M.: Universal dynamic calving law implies potential for abrupt ice-shelf retreat, submitted, 2010. 1309, 1315, 1316

Title Page

Abstract | Introduction

Conclusions | References

Tables | Figures

◄◄ | ►►

◄ | ►

Back | Close

Full Screen / Esc

Printer-friendly Version

Interactive Discussion

Liu, H., Jezek, K. C., and Li, B.: Development of an Antarctic digital elevation model by integrating cartographic and remotely sensed data: a geographic information system based approach, J. Geophys. Res., 104, 23199–23214, 1999. 1319

Lythe, M. B., Vaughan, D. G., and BEDMAP Consortium: BEDMAP: a new ice thickness and subglacial topographic model of Antarctica, J. Geophys. Res., 106, 11335–11351, 2001. 1310, 1316, 1317, 1326

Ma, Y., Gagliardini, O., Ritz, C., Gillet-Chaulet, F., Durand, G., and Montagnat, M.: Enhancement factors for grounded ice and ice-shelves inferred from an anisotropic ice flow model, J. Glaciol., accepted, 2010. 1312, 1313

Oerter, H., Kipfstuhl, J., Determann, J., Miller, H., Wagenbach, D., Minikin, A., and Graft, W.: Evidence for basal marine ice in the Filchner-Ronne ice shelf, Nature, 358, 399–401, 1992. 1311

Paterson, W.: The Physics of Glaciers, Elsevier, Oxford, 1994. 1313

Pollard, D. and Deconto, R. M.: Modelling West Antarctic ice sheet growth and collapse through the past five million years, Nature, 458, 329–332, 2009. 1309, 1310

Pritchard, H. D., Arthern, R. J., Vaughan, D. G., and Edwards, L. A.: Extensive dynamic thinning on the margins of the Greenland and Antarctic ice sheets, Nature, 461, 971–975, 2009. 1308, 1319

Ritz, C., Rommelaere, V., and Dumas, C.: Modeling the evolution of Antarctic ice sheet over the last 420 000 years: implications for altitude changes in the Vostok region, J. Geophys. Res., 106, 31943–31964, 2001. 1309

Schoof, C.: Variational methods for glacier flow over plastic till, J. Fluid Mech., 555, 299–320, 2006a. 1313

Schoof, C. and Hindmarsh, R. C. A.: Thin-film flows with wall slip: An asymptotic analysis of higher order glacier flow models, Q. J. Mech. Appl. Math., 63, 73-114, doi:10.1093/qjmam/hbp025, 2010. 1312

SeaRISE: Sea-level Response to Ice Sheet Evolution (SeaRISE), http://websrv.cs.umt.edu/isis/index.php/SeaRISE_Assessment, last access: 07/30/2010. 1310

Shapiro, N. M. and Ritzwoller, M. H.: Inferring surface heat flux distributions guided by a global seismic model: particular application to Antarctica, Earth Planet. Sc. Lett., 223, 213–224, 2004. 1310

Title Page

Abstract | Introduction

Conclusions | References

Tables | Figures

◀◀ | ▶▶

◀ | ▶

Back | Close

Full Screen / Esc

Printer-friendly Version

Interactive Discussion

Thomas, R., Rignot, E., Casassa, G., Kanagaratnam, P., Acuña, C., Akins, T., Brecher, H., Frederick, E., Gogineni, P., Krabill, W., Manizade, S., Ramamoorthy, H., Rivera, A., Russell, R., Sonntag, J., Swift, R., Yungel, J., and Zwally, J.: Accelerated sea-level rise from West Antarctica, Science, 306, 255–258, 2004. 1319

5 Van de Berg, W. J., Van den Broeke, M. R., Reijmer, C. H., and Van Meijgaard, E.: Reassessment of the Antarctic surface mass balance using calibrated output of a regional atmospheric climate model, J. Geophys. Res., 111, 11104–11119, 2006. 1310

Van den Broeke, M.: Depth and density of the Antarctic firn layer, Arct. Antarct. Alp. Res., 40, 432–438, 2008. 1310

10 Weertman, J.: Stability of the junction of an ice sheet and an ice shelf, J. Glaciol., 13, 3–11, 1974. 1318

Winkelmann, R., Martin, M. A., Haseloff, M., Albrecht, T., Bueler, E., Khroulev, C., and Levermann, A.: The Potsdam Parallel Ice Sheet Model (PISM-PIK) – Part 1: Model description, The Cryosphere Discuss., 4, 1277–1306, doi:10.5194/tcd-4-1277-2010, 2010. 1309, 1311,

15   1312, 1313, 1316, 1328

PISM-PIK – Part 2

M. A. Martin et al.

Title Page

Abstract	Introduction
Conclusions	References
Tables	Figures

|◄ | ►|

◄ | ►

Back | Close

Full Screen / Esc

Printer-friendly Version

Interactive Discussion

Table 1. Table of symbols and values of constants.

Symbol	Description	SI units	Value
b	bedrock elevation	m	
C	calving rate	$m\,s^{-1}$	
c_{p_o}	specific heat capacity of ocean mixed layer	$J\,(kg\,K)^{-1}$	3974
E_{SIA}	enhancement factor for the SIA		4.5
E_{SSA}	enhancement factor for the SSA		$\sqrt[n]{0.8}\approx0.93$
F_{melt}	parameter for subshelf melting	$m\,s^{-1}$	5×10^{-3}
G	geothermal flux	$W\,m^{-2}$	
g	acceleration due to gravity	$m\,s^{-2}$	9.81
h	upper surface elevation of ice	m	
H	ice thickness	m	
H_c	ice thickness at calving front	m	
$\{i,j\}$	2d horizontal tensor indices		
K	proportionality constant for Eigen Calving	$m\,s$	10^{19}
L_i	latent heat capacity of ice	$J\,kg^{-1}$	3.35×10^5
n	Glen flow law exponent		3
p_w	pore water pressure	$N\,m^{-2}$	
Q	horizontal ice flux	$m^2\,s^{-1}$	
S	ice equivalent basal mass balance ($S>0$ is melting)	$m\,s^{-1}$	
S_o	salinity of ocean water under ice shelves	psu	35
T	ice temperature	K	
T_f	freezing temperature	K	
T_s	surface temperature	K	
T_o	temperature of ocean water	K	271.45 ($-1.7\,^\circ$C)
T_{pm}	pressure-melting temperature	K	
$\boldsymbol{v}$	overall horizontal ice velocity	$m\,s^{-1}$	
$\boldsymbol{v}_b$	basal ice velocity; $\boldsymbol{v}_b=\boldsymbol{v}_{SSA}=(v_x,v_y)$	$m\,s^{-1}$	
$\boldsymbol{v}_{SIA}$	SIA-modeled velocity of ice	$m\,s^{-1}$	
$\boldsymbol{v}_{SSA}$	SSA-modeled velocity of ice; $\boldsymbol{v}_{SSA}=(v_x,v_y)$	$m\,s^{-1}$	
(x,y)	horizontal dimensions	m	
z	vertical dimension (positive upwards)	m	
z_b	elevation of the ice shelf base	m	
z_{sl}	sea level	m	0
β_{CC}	Clausius-Clapeyron gradient	$K\,m^{-1}$	8.66×10^{-4}
γ_T	thermal exchange velocity	$m\,s^{-1}$	10^{-4}
$\Delta x, \Delta y$	horizontal grid size	km	19.98
$\dot{e}_\pm$	eigenvalues of horizontal strain rate tensor	s^{-1}	
λ	parameter for water content in till		
ρ_i	density of ice	$kg\,m^{-3}$	910
ρ_o	density of ocean water	$kg\,m^{-3}$	1025
τ_b	basal shear stress on ice	$Pa=N\,m^{-2}$	
τ_c	yield stress	$Pa=N\,m^{-2}$	
τ_{ij}	deviatoric stress tensor; $\tau_{ij}=2v\dot{e}_{ij}$	$Pa=N\,m^{-2}$	
ϕ	till friction angle	$^\circ$	
$|\Phi|$	latitude	$^\circ$S	

Table 2. Comparison with observations of key quantities in the PISM-PIK dynamical equilibrium simulation (Lythe et al., 2001; Le Brocq et al., 2010). The column labeled "difference" is the amount by which the model result exceeds observations.

Quantity	Observations	PISM-PIK	Difference
Total ice volume	$256 \times 10^{14}\,\mathrm{m}^3$	$259 \times 10^{14}\,\mathrm{m}^3$	+1.2 %
Grounded ice volume	$249 \times 10^{14}\,\mathrm{m}^3$	$255 \times 10^{14}\,\mathrm{m}^3$	+2.4 %
Total ice area	$137 \times 10^{11}\,\mathrm{m}^2$	$136 \times 10^{11}\,\mathrm{m}^2$	−0.7 %
Grounded ice area	$123 \times 10^{11}\,\mathrm{m}^2$	$125 \times 10^{11}\,\mathrm{m}^2$	+1.6 %
Floating ice area	$143 \times 10^{10}\,\mathrm{m}^2$	$111 \times 10^{10}\,\mathrm{m}^2$	−22.4 %
Ice front type: marine	28%	54%	–
Ice front type: cliff	25%	24%	–
Ice front type: shelf	47%	22%	–
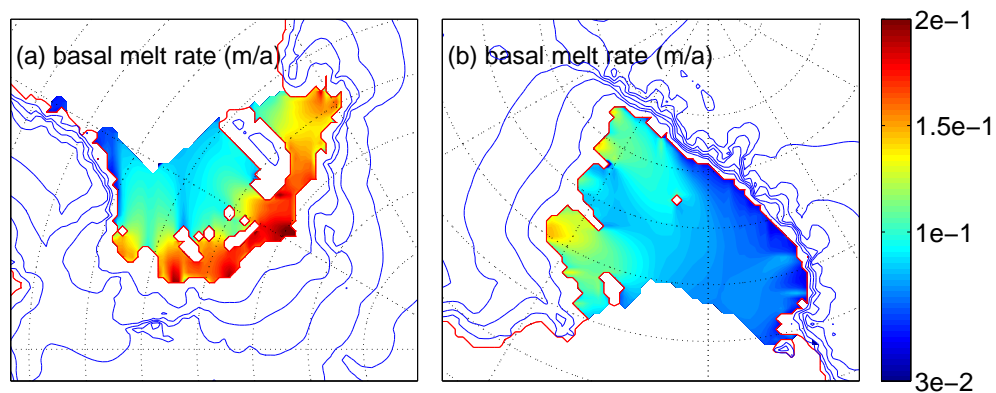
Fig. 1. Basal melt rate for **(a)** Ronne-Filchner and **(b)** Ross Ice Shelves, as given by Eq. (7). The parameterization used here leads to melt rates which depend on the shelf thickness and are highest near the grounding lines (red). Blue lines are contours of surface elevation.

Title Page

Abstract   Introduction

Conclusions   References

Tables   Figures

◄◄   ►►

◄   ►

Back   Close

Full Screen / Esc

Printer-friendly Version

Interactive Discussion
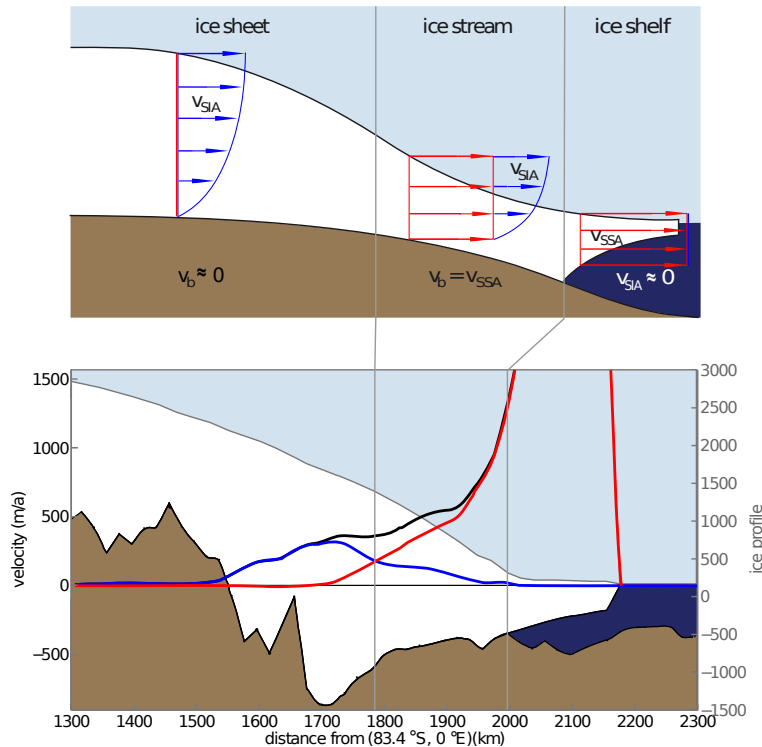
Fig. 2. Superposition of SIA and SSA velocities. Upper panel: a schematic diagram of an ice profile showing the different flow regimes in PISM-PIK. Repeats Fig. 1 from Winkelmann et al. (2010). Lower panel: an example cut through the sheet-stream-shelf transition of the Lambert Glacier and Amery Ice Shelf in the simulation. The location is shown by the green line in Fig. 7. The onset of an ice stream is diagnosed to be where the basal sliding velocity v_b (red curve) exceeds the SIA velocity v_{SIA} (blue curve). The model output velocity $v = v_b + v_{SIA}$ is shown in black.

Title Page

Abstract | Introduction

Conclusions | References

Tables | Figures

◄◄ | ►►

◄ | ►

Back | Close

Full Screen / Esc

Printer-friendly Version

Interactive Discussion
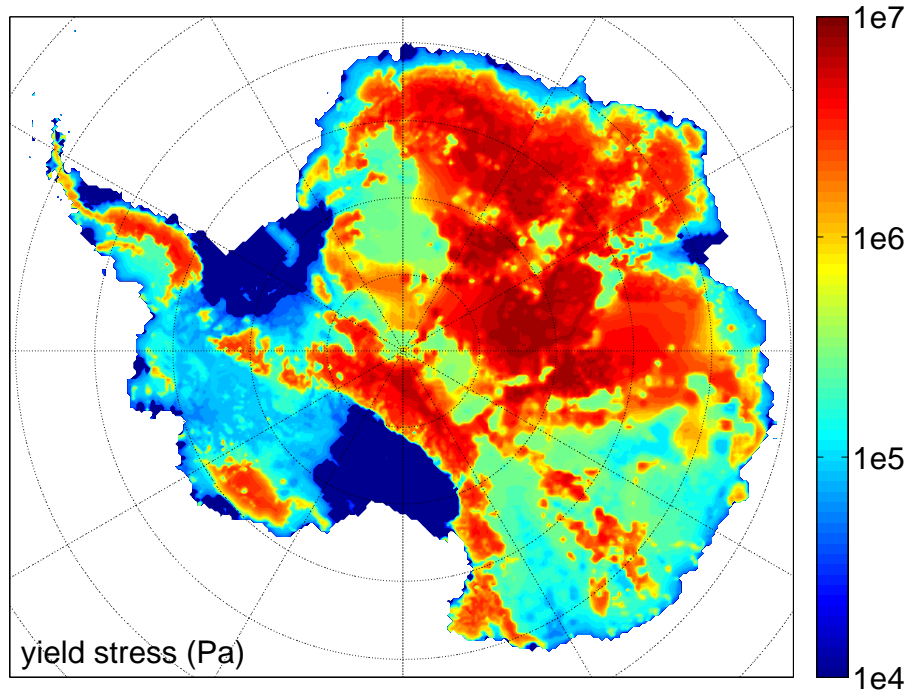
Fig. 3. Map of yield stress τ_c, following Eqs. (10–13).

Fig. 4. Eigen Calving law applied to **(a)** Ronne-Filchner and **(b)** Ross Ice Shelves. Blue shading represents the spreading rate $\dot{e}_+$ along the main flow direction, white lines (zero line of $\dot{e}_-$) illustrate possibly weak shelf regions where transversal spreading occurs. (Grounding line is represented by red line, onset of streams by black lines.)
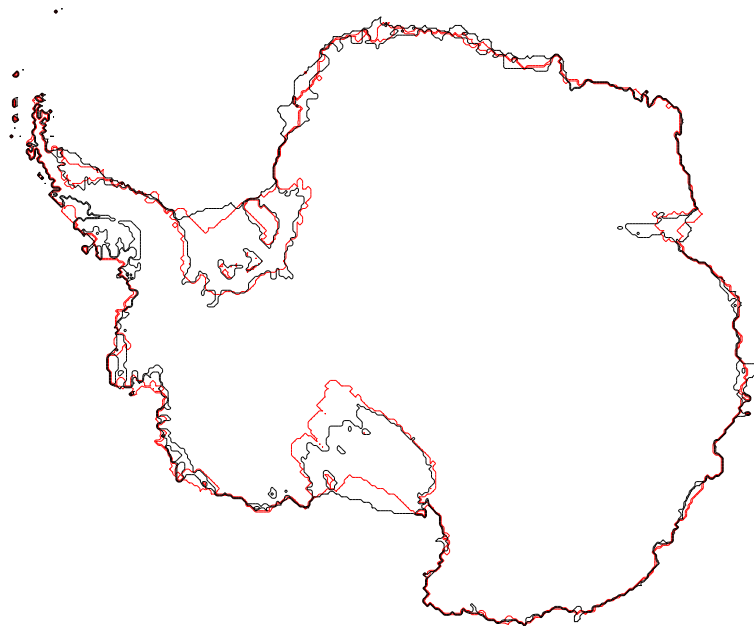
Fig. 5. Comparison of grounding-line and ice-front positions from ALBMAP dataset (black) and PISM-PIK dynamic equilibrium simulation (red).
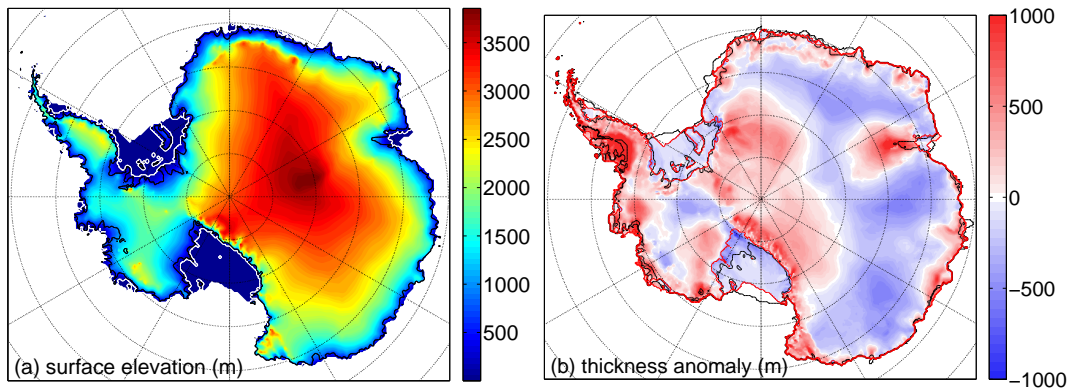
Fig. 6. (a) Surface elevation in model equilibrium. **(b)** Difference in ice thickness: dynamic equilibrium simulation minus ALBMAP data. Red indicates model overestimation of ice thickness while blue is underestimation.
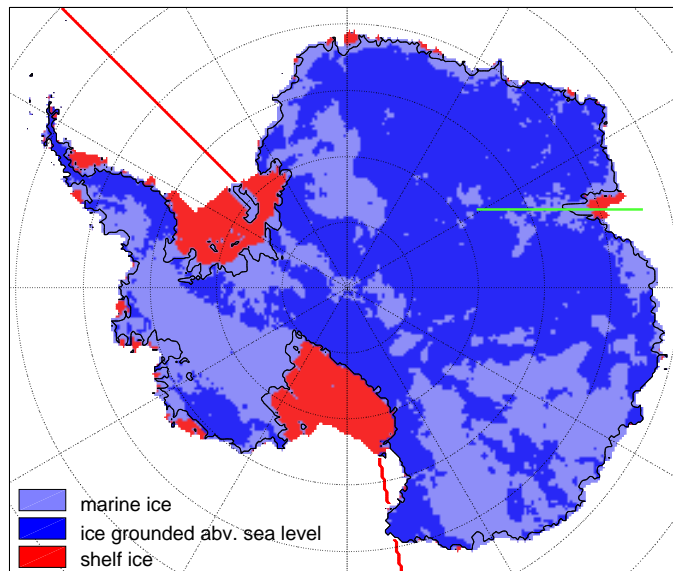
Fig. 7. Modeled distribution of different types of ice grid cells: Shelves are red, ice grounded above sea level is blue and ice grounded below sea level (marine ice) is light blue. The onset of ice streams, diagnosed by inequality Eq. (8), is outlined in black. The green line indicates the cut through the sheet-shelf transition zone in the Amery region shown in profile in Fig. 2. The red lines along 45° W and 169° E longitude, respectively, indicate the partitioning of the ice sheet into West Antarctica and East Antarctica.
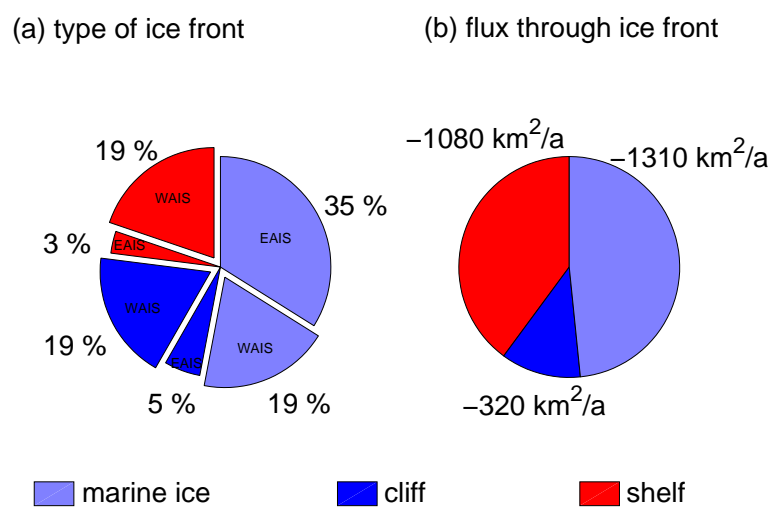
Fig. 8. **(a)** Partitioning of the different types of ice fronts in the equilibrium simulation, and **(b)** their contribution to the mass budget. Note that an ice flux of $-1230\,\text{km}^2/\text{a}$ can be attributed to East Antarctica.
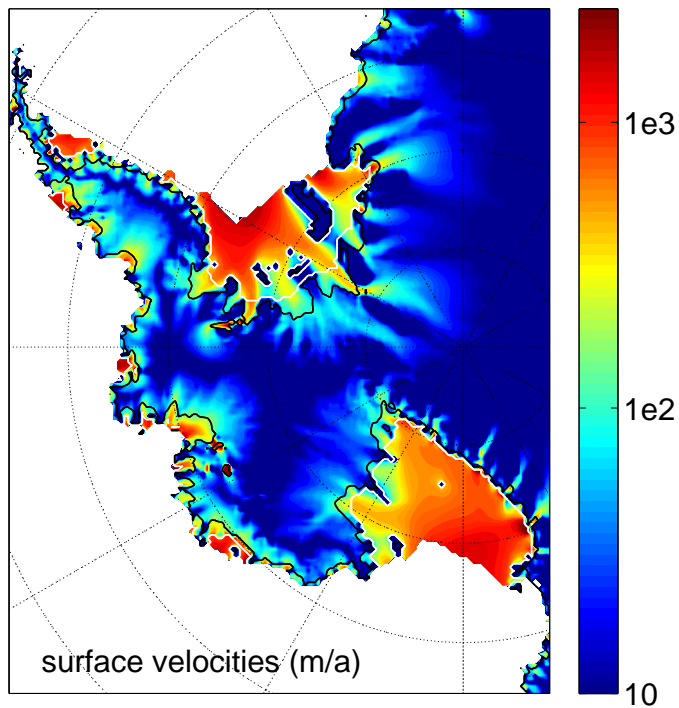
Fig. 9. Modeled surface velocity for the West Antarctic Ice Sheet. White lines show the grounding-line position, thin black lines indicate ice streams according to inequality Eq. (8).

Title Page

Abstract | Introduction

Conclusions | References

Tables | Figures

|◄ | ►|

◄ | ►

Back | Close

Full Screen / Esc

Printer-friendly Version

Interactive Discussion
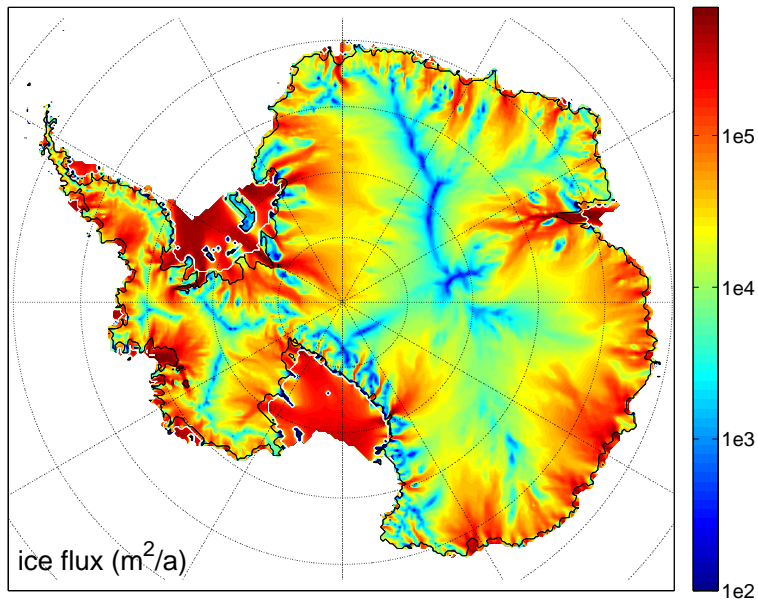
Fig. 10. Modeled ice flux. Ice streams are outlined in black, grounding line position in white.

Title Page

Abstract	Introduction
Conclusions	References
Tables	Figures

|◄ ►|

◄ ►

Back Close

Full Screen / Esc

Printer-friendly Version

Interactive Discussion
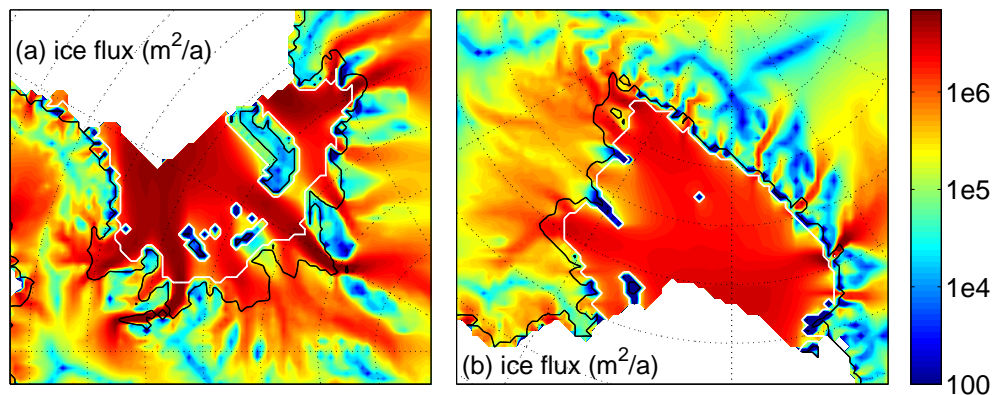
Fig. 11. Ice flux with streams indicated by black line for **(a)** Ronne-Filchner and **(b)** Ross Ice Shelves. The grounding line is marked by a white line.
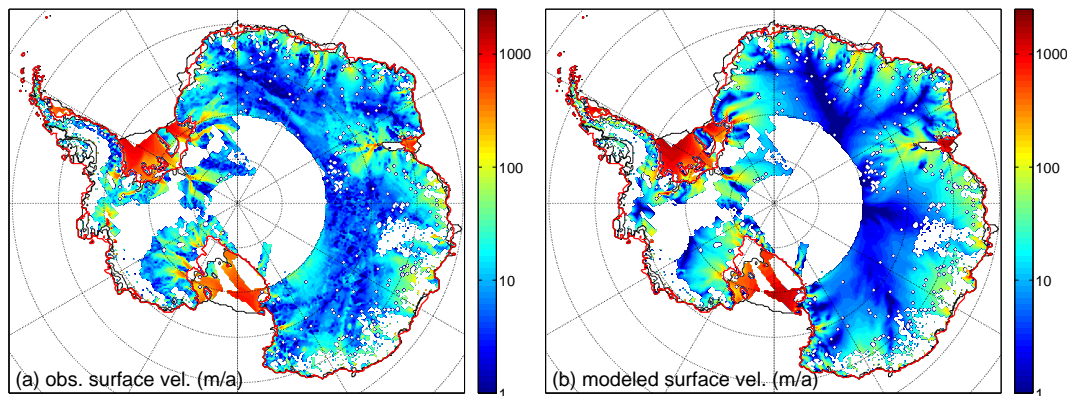
Fig. 12. Comparison of surface velocity fields. **(a)** Observed surface velocities from MAMM data enriched by data from Joughin et al. (2002). **(b)** Surface velocities from equilibrium simulation. In both (a) and (b), regions without observational coverage and where there is no agreement in the simulation and the observations about whether the ice is grounded or floating are masked out, which leaves 65% of total ice covered area for comparison. The respective grounding line positions and calving fronts for observation and model are depicted in black and red, as in Fig. 5.
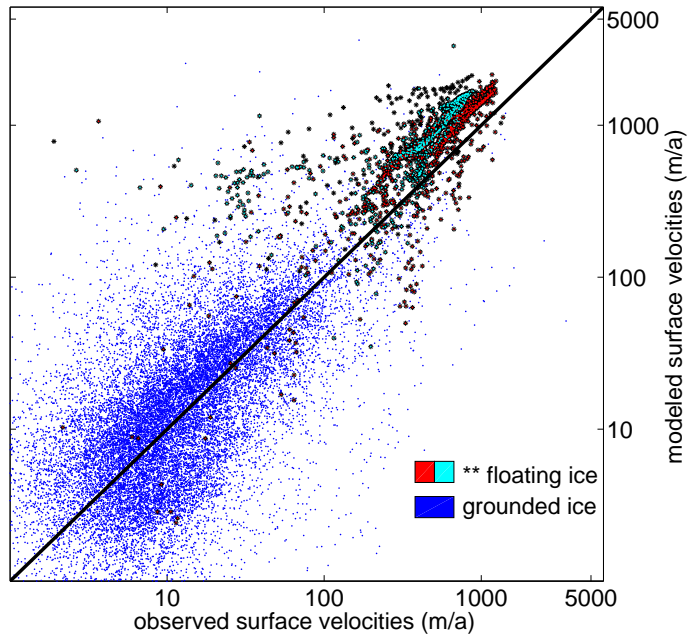
Fig. 13. Point-by-point scatterplot of modeled and observed velocities. The mean difference from modeled to observed velocities for grounded points is ≈4 m/a with a standard deviation from this mean difference of ≈80 m/a. For floating points we get a larger difference of ≈330 m/a with a standard deviation of ≈280 m/a. The stars with red points are the floating velocities that belong to the Ronne-Filchner Ice-Shelf, while the ones with the cyan points belong to the Ross Ice Shelf.
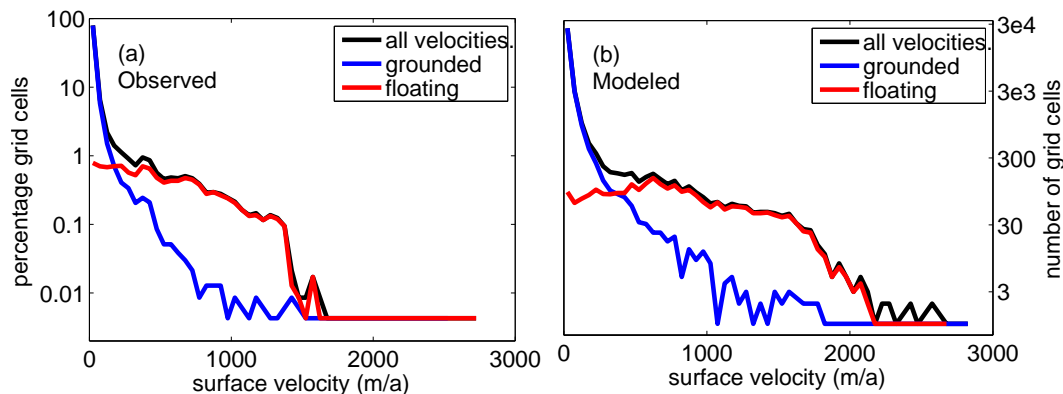
Fig. 14. Histogram of velocity distribution. **(a)** observed **(b)** modeled. Each of 60 bins contains a velocity range of $\Delta v_{surface} = 50\,\mathrm{m\,a}^{-1}$.
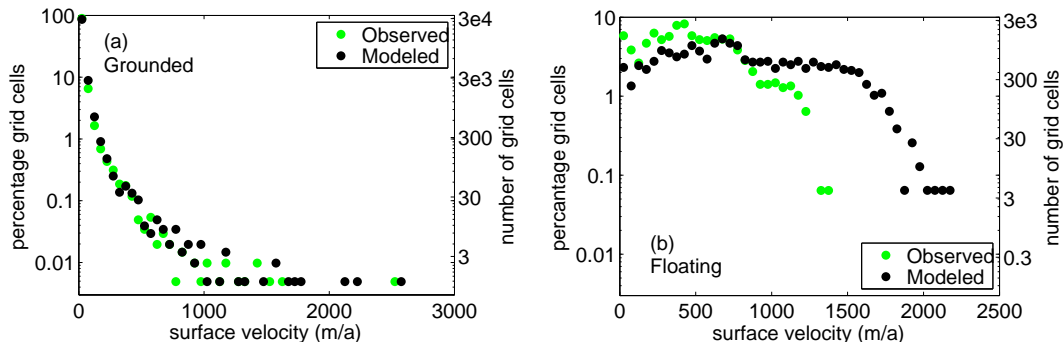
Fig. 15. Histogram of velocity distribution. Panel **(a)** grounded and panel **(b)** floating areas (please note that the strongest overestimation occurs only for a small number of grid cells). Relative Fig. 14, we show results from the smaller dataset (Fig. 12), containing only data where there is agreement between model and observation about whether the ice is grounded or floating.